Liver INTERNATIONAL

Liver International ISSN 1478-3223

CANCER

Clinicopathological indices to predict hepatocellular carcinoma molecular classification

Poh Seng Tan[1,2,*], Shigeki Nakagawa[1,*], Nicolas Goossens[1,3,*], Anu Venkatesh[1], Tiangui Huang[4], Stephen C. Ward[4], Xiaochen Sun[1], Won-Min Song[5], Anna Koh[1], Claudia Canasto-Chibuque[1], Manjeet Deshmukh[1], Venugopalan Nair[6], Milind Mahajan[5], Bin Zhang[5], Maria Isabel Fiel[4], Masahiro Kobayashi[7], Hiromitsu Kumada[7] and Yujin Hoshida[1]

1 Division of Liver Diseases, Department of Medicine, Liver Cancer Program, Tisch Cancer Institute, Icahn School of Medicine at Mount Sinai, New York, NY, USA
2 Division of Gastroenterology and Hepatology, University Medicine Cluster, National University Health System, Singapore, Singapore
3 Division of Gastroenterology and Hepatology, Geneva University Hospital, Switzerland
4 Department of Pathology, Icahn School of Medicine at Mount Sinai, New York, NY, USA
5 Department of Genetics and Genomic Sciences, Icahn School of Medicine at Mount Sinai, New York, NY, USA
6 Department of Neurology, Icahn School of Medicine at Mount Sinai, New York, NY, USA
7 Department of Hepatology, Toranomon Hospital, Tokyo, Japan

Liver Int. 2016; 36: 108–118. DOI: 10.1111/liv.12889

Abstract

Background & Aims: Hepatocellular carcinoma (HCC) is the second most lethal cancer caused by lack of effective therapies. Although promising, HCC molecular classification, which enriches potential responders to specific therapies, has not yet been assessed in clinical trials of anti-HCC drugs. We aimed to overcome these challenges by developing clinicopathological surrogate indices of HCC molecular classification. *Methods:* Hepatocellular carcinoma classification defined in our previous transcriptome meta-analysis (S1, S2 and S3 subclasses) was implemented in an FDA-approved diagnostic platform (Elements assay, NanoString). Ninety-six HCC tumours (training set) were assayed to develop molecular subclass-predictive indices based on clinicopathological features, which were independently validated in 99 HCC tumours (validation set). Molecular deregulations associated with the histopathological features were determined by pathway analysis. Sample sizes for HCC clinical trials enriched with specific molecular subclasses were determined. *Results:* Hepatocellular carcinoma subclass-predictive indices were steatohepatitic (SH)-HCC variant and immune cell infiltrate for S1 subclass, macrotrabecular/compact pattern, lack of pseudoglandular pattern, and high serum alpha-foetoprotein (>400 ng/ml) for S2 subclass, and microtrabecular pattern, lack of SH-HCC and clear cell variants, and lower histological grade for S3 subclass. Macrotrabecular/compact pattern, a predictor of S2 subclass, was associated with the activation of therapeutically targetable oncogene *YAP* and stemness markers *EPCAM/KRT19*. *BMP4* was associated with pseudoglandular pattern. Subclass-predictive indices-based patient enrich-

Abbreviations

AFP, alpha-foetoprotein; AUROC, area under receiver operating characteristic; BCLC, Barcelona Clinic Liver Cancer; FDR, false discovery rate; FFPE, formalin-fixed paraffin-embedded; GSEA, Gene Set Enrichment Analysis; H&E, hematoxylin and eosin; HBV, hepatitis B virus; HCC, hepatocellular carcinoma; HCV, hepatitis C virus; KDA, Key Driver Analysis; NAFLD, non-alcoholic fatty liver disease; NASH, non-alcoholic steatohepatitis; NNT, number needed to treat; NPV, negative predictive value; OR, odds ratio; ORR, objective response rate; PFNA, Planar Filtered Network Analysis; PPV, positive predictive value; SH-HCC, steatohepatitic hepatocellular carcinoma.

Correspondence

Yujin Hoshida, MD, PhD, Division of Liver Diseases, Department of Medicine, Liver Cancer Program, Tisch Cancer Institute, Icahn School of Medicine at Mount Sinai, 1470 Madison Ave, Box 1123, New York, NY 10029, USA
Tel: +1 212 824 8862; Fax: +1 646 537 9576
e-mail: yujin.hoshida@mssm.edu

*Contributed equally to this work.

Microarray data are available at NCBI Gene Expression Omnibus (GSE59548)

Correction added after first online publication on Sep 29, 2015: Maria Isabel Fiel's affiliation has been corrected.

Handling Editor: Morris Sherman

Received 27 February 2015; Accepted 1 June 2015

Additional Supporting Information may be found at onlinelibrary.wiley.com/doi/10.1111/liv.12889/suppinfo

Key points

- An HCC molecular classification test was implemented in a clinically applicable, FDA-approved assay platform, and successfully validated in an independent patient cohort.
- Clinicopathological indices predictive of HCC molecular classification were developed and validated.
- Deregulated molecular pathways tightly associated with specific histopathological features of HCC tumour were comprehensively catalogued, e.g. activation of oncogene YAP and stemness markers EPCAM/KRT19 in macrotrabecular/compact pattern and BMP4 overexpression, known to be involved in gland formation in kidney, in pseudoglandular pattern.
- The clinically applicable HCC molecular classification assay and predictive indices will facilitate further evaluation of clinical utility of HCC molecular subclasses and personalized therapeutic development.

ment reduced clinical trial sample sizes from 121, 184 and 53 to 30, 43 and 22 for S1, S2 and S3 subclass-targeting therapies respectively. *Conclusions:* Hepatocellular carcinoma molecular subclasses can be enriched by clinicopathological indices tightly associated with deregulation of therapeutically targetable molecular pathways.

Keywords
clinical diagnostic – gene expression – histopathology – molecular subclass – predictive index

Liver cancer, mainly hepatocellular carcinoma (HCC), is the second leading cause of cancer death worldwide, and its prognosis is still dismal (5-year survival rate generally below 15%) (GLOBOCAN 2012, globocan.iarc.fr). Underlying chronic liver disease, namely cirrhosis, serves as a fertile soil for *de novo* carcinogenesis, therefore early detection and complete removal or ablation of the tumours rarely prevents tumour recurrence (1). Once the tumours reach advanced stage as a consequence of multiple rounds of *de novo* carcinogenesis, only one approved medical therapy is available, sorafenib, which extends patient survival by only 3 months (2, 3). The development of improved HCC therapies has been challenging as evidenced by the series of failed phase 3 trials of various molecular targeted agents (4). It is increasingly emerging that this is attributable to the lack of predictive biomarker of response to enrich potential responders to detect therapeutic benefit in clinical trials (4).

Genomics studies in the past decade have elucidated numerous therapeutic targets, which can be mapped onto the framework of HCC molecular classification defined in our previous transcriptome meta-analysis of global HCC populations from Asia, Europe and the U.S., including more than 600 patients (named S1, S2 and S3 subclasses) and independently validated (5–8). The molecular hallmarks of the HCC subclasses have become increasingly targetable by newly developed therapies. For example, inhibitors of TGF-beta pathway (a hallmark of S1), glypican-3 (a marker of S2) and MET pathway (S1/S2) have been evaluated in recent early-stage clinical trials in HCC (9–11). Alpha-foetoprotein (AFP), a marker of S2 tumours, was targeted by AFP genetic vaccine (12). A *Src/Abl* inhibitor, dasatinib, showed preferential effect in S1-like hepatoma cell lines (13, 14). We recently found that siRNA-based silencing of *YAP* oncogene (activated in S2 subclass) induced HCC tumour regression (15). These studies collectively suggest that determination of HCC molecular subclass may serve as a broadly applicable predictive biomarker of response to these therapies.

Given that the latest clinical practice guidelines recommend tumour tissue biopsy in the setting of therapeutic clinical trials (16), tools to inexpensively and robustly determine the molecular subclasses and aberrations in clinical specimens are urgently needed. However, such molecular subclass/biomarker-enriched clinical trials have been rarely conducted because of financial constraints in the biomarker component of clinical trials. In addition, although such molecular classification could refine clinical patient management by informing patient prognosis, it is still challenging to disseminate the information widely because the vast majority of HCC patients are diagnosed in developing, resource-poor countries, where the implementation of molecular biomarker assays is practically infeasible (8).

To overcome these challenges, here we aimed to develop and validate clinically readily available surrogates of HCC molecular classification based on robust clinicopathological information, which enables clinical

trial enrichment for molecular targeted anti-HCC drugs. Furthermore, we implemented and evaluated a gene signature-based HCC molecular classification assay in an FDA-approved diagnostic platform applicable to clinical archived formalin-fixed, paraffin-embedded (FFPE) tissues (17). The assay may be used to retrospectively corroborate the clinicopathological indices-based subclass prediction whenever funding and/or access to the assay facility become available in a real-world clinical setting. Of note, the assay provides objective readout unlike immunohistochemistry, which relies on molecular pathology expertise and somewhat subjective interpretation, using exactly the same material, i.e. FFPE tissue sections. Collectively, the information of HCC molecular classification will become globally accessible to facilitate therapeutic development and refined patient care.

Patients and methods

Patient cohorts

Archived FFPE tissues from 96 tumour foci from 88 HCC patients who underwent surgical resection between 1992 and 2012 at Toranomon Hospital were used for development of clinicopathological indices predictive of HCC molecular subclasses (training set) (Fig. S1). The predictive indices were validated in an independent set of 99 HCC patients, for which the molecular subclasses were determined based on genome-wide transcriptome profiling in our previous study (5), and analyzable hematoxylin and eosin (H&E)-stained FFPE tissue sections were available (validation set). Hepatitis C virus (HCV) infection was determined by positivity of serum HCV antibody or RNA. Hepatitis B virus (HBV) infection was determined by positivity of the hepatitis B surface antigen (HBsAg). Alcohol abuse was defined as lifetime alcohol intake greater than 500 kg. Non-alcoholic fatty liver disease (NAFLD) and non-alcoholic steatohepatitis (NASH) were diagnosed according to current practice guidelines (18). The study, retrospectively analyzing archived tissues from previous treatment performed as routine clinical care, was approved and acquisition of written informed consent was waived by the institutional review board granted on the condition that all samples were anonymized. The study protocol conforms to the ethical guidelines of the 1975 Declaration of Helsinki as reflected in *a priori* approval by the institution's human research committee [Program for the Protection of Human Subjects (PPHS)].

Histopathological analysis

Histopathological evaluation of representative H&E stained slides was independently performed by three pathologists (T.H., S.C.W. and M.I.F.), three hepatologists (P.T., N.G. and Y.H.) and one liver surgeon (S.N.) with liver pathology training. All evaluators were blinded to information of the molecular subclass. Discrepant readings (observed in 17 tumours, 9%) were reconciled by discussion of the six evaluators. Foci within the tumours were classified based on architecture and cytological features according to the World Health Organization Classification of Tumours of the Digestive System (4th edition) and related publications (19–21). The following histological patterns and cytological variant were determined: microtrabecular pattern, macrotrabecular pattern, compact

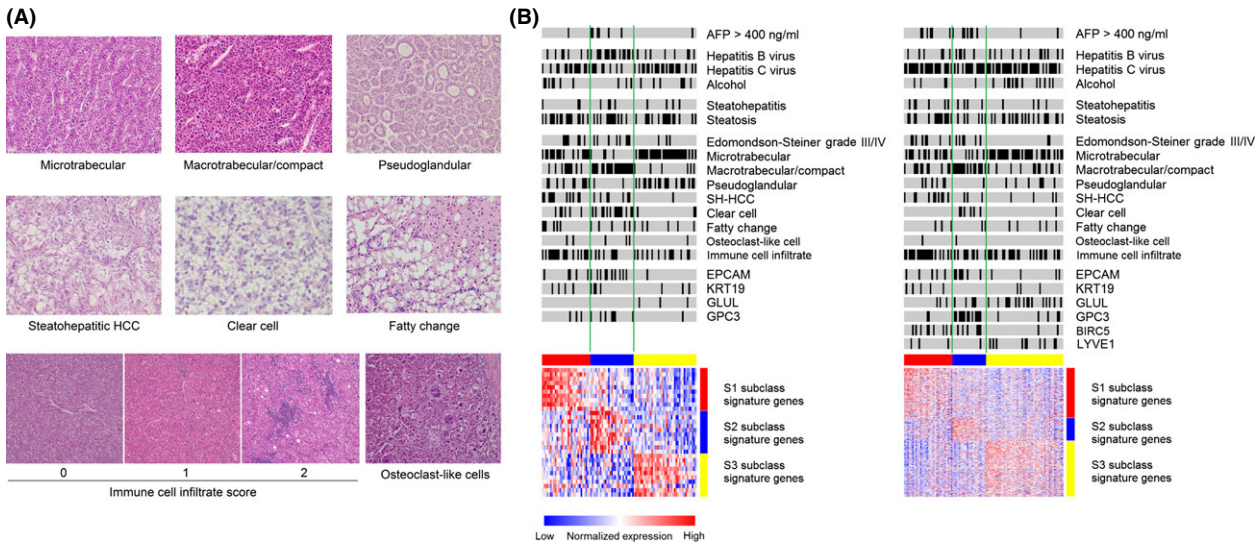

Fig. 1. (A) Histopathological features of HCC tumours. Architectural patterns and cytological variants analyzed for correlation with HCC molecular subclasses. (B) HCC molecular subclasses and clinicopathological features in the training (left) and validation (right) sets. Black bars indicate positivity of the feature. HCC tumours with high immune cell infiltrate (score of 2) are shown by black bars. Red, blue and yellow colours in the horizontal bars above the heatmaps indicate S1, S2 and S3 tumours respectively. Red and blue colours in the heatmaps indicate high and low gene expression respectively.

pattern, pseudoglandular pattern, clear cell variant, steatohepatitic HCC (SH-HCC) variant, and fatty change (Fig. 1A). The trabecular pattern was characterized by cords of tumour cells separated by sinusoidal-like vascular spaces, which was further classified into the microtrabecular pattern if the cords were composed of up to 10 cells (mostly 3–5 cells) and the macrotrabecular pattern if the cords were thicker than 10 cells without endothelial cells between the cords. The compact pattern was characterized by extensive compression of the sinusoidal spaces resulting in its solid appearance. The pseudoglandular pattern was characterized by the presence of gland-like structures that represent dilated, abnormal bile canaliculi surrounded by a ring of tumour cells. The clear cell variant was characterized by uniform tumour cells with centrally located nuclei and prominent optically clear cytoplasm, attributed to glycogen accumulation, without obvious vesicles or other cytoplasmic structures (22–24). The steatohepatitic HCC (SH-HCC) variant is a recently described HCC variant that is characterized by tumour cells showing ballooning degeneration-like appearance often accompanied by cytoplasmic lipid droplets, Mallory-Denk bodies, pericellular fibrosis, and/or inflammatory infiltrates (25–27). Fatty change was characterized by tumour cells with large cytoplasmic lipid-containing vacuoles that displace the nucleus to the periphery and without the features of SH-HCC variant. Foci of tumour cells forming clear subnodules/subcomponents with distinct histological patterns from other components within a tumour nodule were dissected and separately analyzed for transcriptome profiling. The histological features present in more than 30% of each profiled area were recorded and correlated with the molecular subclasses. Histological grading was determined according to the Edmondson-Steiner grading system on an entire HCC nodule (28). Steatosis and steatohepatitis in non-tumour liver were determined by greater than 5% steatosis and presence of ballooning degeneration respectively (29). Immune cell infiltrate within the tumour was scored 0–2 according to the mean number of infiltrating lymphocytes from 5 high-powered fields (0: 0–5 cells, 1: 5–20 cells, 2: >20 cells) (30). A recently described HCC variant, chromophobe HCC as well as osteoclast-like cell were also assessed (31, 32).

Transcriptome-based determination of HCC molecular subclasses

To determine the S1, S2, and S3 subclasses, we implemented a classifier gene signature, originally comprised of 619 genes, in the digital transcript counting technology (Elements assay, NanoString), an FDA-approved clinical diagnostic platform capable of analyzing severely degraded FFPE RNA (17). Because the number of gene probes is the major determinant of the assay cost, we first bioinformatically evaluated performance of the top informative HCC molecular subclass signature genes that fit the minimum unit of Elements assay (30 signature genes and 6 normalization genes). From among the 619 full HCC subclass signature genes already verified for their subclass predictive performance in our previously reported random resampling-based transcriptome meta-analysis of nine independent HCC data sets (5), top 30 genes (10 genes for each subclass) with the largest Fisher's inverse chi-square were chosen for the assay development (30-gene signature, Table S1). The subclass prediction was repeated with the 30-gene signature in the nine independent HCC data sets (Table S2) using nearest template prediction algorithm as previously described (5), and concordance with the original prediction made by the 619-gene signature was evaluated. We observed an overall concordance of 85% (IQR: 80–90%, range: 72–94%) (Fig. S2). Prediction concordance for S1, S2, and S3 subclasses were 79% (IQR: 74–88%), 85% (IQR: 82–93%), and 87% (IQR: 84–89%) respectively. Based on these results, indicating that the 30-gene signature enables reasonably reproducible determination of HCC molecular subclass, we implemented the signature in the elements assay platform.

Total RNA was isolated from three 10-micron-thick FFPE tissue sections by using High Pure RNA Paraffin Kit (Roche, New York, NY, USA). Multiple histopathological foci co-existing in a tumour nodule were macro-dissected based on serial H&E stained section. Expression profiling was performed using 100–500 ng total RNA samples with nCounter Analysis System (NanoString, Seattle, WA, USA). Raw scan data were extracted by NSOLVER software ver.1 (NanoString, Seattle, WA, USA), and normalized by scaling with geometric mean of normalization gene probes by using NanoString normalizer module of GenePattern genomic analysis toolkit (www.broadinstitute.org/genepattern). The data sets are available at NCBI Gene Expression Omnibus (GEO) database (GSE59548, GSE10186).

Expression of HCC marker genes

Expression of previously documented stemness marker genes in HCC, *KRT19* and *EPCAM*, as well as a marker gene of *CTNNB1* exon 3-mutated HCC tumours, *GLUL* (33), were determined by reverse transcription quantitative polymerase chain reaction RT-qPCR in the training set. Total RNA was converted into cDNA using EcoDry Premix (Clontech Laboratories, Mountain View, CA, USA) on Matercycler Nexus Gradient (Eppendorf, Hauppauge, NY, USA), and qPCR was performed using iQ SYBR Green Supermix (Bio-Rad, Hercules, CA, USA) on CFX384 Touch Real-Time PCR Detection System (Bio-Rad, Hercules, CA, USA) following manufacturer's instruction. Used primer sequences are summarized in Table S3. Gene expression level was calculated using delta-delta Ct method based on a housekeeping gene, *RPL13A*. Tumours were classified into high- or low-expression group based on one standard deviation above mean.

Bioinformatics analysis

Molecular pathway deregulations associated with the histopathological features were determined in the genome-wide transcriptome data set of the validation set by surveying a comprehensive collection of 10 295 annotated pathway gene sets in Molecular Signature Database (MSigDB, www.broadinstitute.org/mdigdb) and a collection of liver cancer-related gene signatures in literature (Table S4) using Gene Set Enrichment Analysis (GSEA) (34). Functionally co-regulated gene networks in association with the histopathological features were determined by using Planar Filtered Network Analysis (PFNA) algorithm (35). Briefly, global gene co-expression network was first constructed by using the genome-wide profiles of the validation set based on Pearson correlation coefficient. Co-regulated gene modules (subnetworks) with significant and robust biological/functional links were subsequently determined on a hyperbolic surface (36, 37). Gene modules associated with each of the histopathological features were determined by using GSEA of the module member genes on gene list in the validation transcriptome data set rank-ordered according to differential expression between tumours with the feature and the rest by using random permutation t-test implemented in GenePattern. Key regulatory genes in the gene modules associated with each of the histopathological features were determined by Key Driver Analysis (KDA), which prioritizes driver genes by measuring the impact on the down-stream genes such that the down-stream genes were defined by n-layer neighbourhood in a co-expression network with optimal n that maximizes the enrichment statistic (38). When adjustment for high-dimensional multiple hypothesis testing was needed, Benjamini-Hochberg false discovery rate (FDR) <0.05 was regarded as statistically significant. All analyses were performed using GenePattern and R statistical language (www.r-project.org).

Statistical analysis

Categorical and unpaired continuous data were tested by Fisher's exact test and Wilcoxon rank-sum test respectively. Logistic regression was used to evaluate correlation between each HCC molecular subclass and the clinicopathological features (architectural patterns, cytological variants, tumour grade, microvascular invasion, presence of satellite lesions, tumour size, multiplicity, serum AFP level, AFP lens culinaris agglutinin-reactive fraction 3 [L3], and des-gamma-carboxy prothrombin [DCP]), the HCC molecular markers (*KRT19*, *EPCAM*, and *GLUL*), and disease aetiologies (HBV, HCV, alcohol, and NAFLD). Variables with $P < 0.05$ in univariable analysis were further evaluated in multivariable logistic regression modelling with stepwise variable selection for the development of HCC molecular subclass-predictive indices using the regression coefficients. Given that the patency of sinusoidal-like spaces within a tumour could be artificially modified during the process of tissue fixation and processing, we combined the macrotrabecular and compact patterns into a single composite variable for the correlation analysis. Two sets of cut-off values for the HCC molecular subclass-predictive indices were determined based on receiver operating characteristic (ROC) curves in the training set to maximize either (i) positive predictive value (PPV) to examine the scenarios of clinical trial enrichment or (ii) sensitivity/specificity to determine diagnostic performance of the indices in general, and applied to the validation set. Sample size required to detect a therapeutic response in clinical trials of anti-HCC drugs targeting each of the HCC molecular subclasses was calculated based on alpha error of 0.05, power of 0.90, and treatment/control ratio of 1. Objective response rate (ORR) in molecularly determined targeted subclass was assumed to range from 50% to 70% based on published lung cancer trials enriched with *EGFR* gene mutations- or *ALK* gene fusion-positive patients (39). Given the scenario that HCC patients predicted to have the target subclass using the clinicopathological indices are enrolled into clinical trials, PPVs derived from the validation set were used to calculate proportion of patients with true targeted molecular subclass. Prevalence of S1, S2, and S3 subclasses were assumed to be 30%, 25%, and 45%, respectively, from the prevalence in the current training and validation sets and our previous study (5). Number needed to treat (NNT) was calculated based on the same assumption on ORR and PPV. Two-tailed P-value <0.05 was considered as statistically significant. All analyses were performed using R statistical language.

Results

Patients

Patients in the validation set were slightly younger and more frequently affected with HCV infection compared to the training set (Table 1). Three patients in the training set had a definite diagnosis of NAFLD/NASH as a sole aetiology of HCC. Serum bilirubin was marginally higher in the validation set but still within the normal reference range. There was no significant difference in the proportion of tumours with AFP level greater than 400 ng/ml. More than 90% of the tumours were stage 0/A in both the training and validation sets.

Histopathological features of HCC tumours

The micro/macrotrabecular, compact, and pseudoglandular patterns, SH-HCC, clear cell, immune cell infiltrates, and fatty change were present in more than 5% of the tumours in both training and validation sets, ascertaining general applicability of the analyzed features (Table 2). Diagnostic concordance among the three pathologists was greater than 70% for all the histo-

Table 1. Clinical characteristics of HCC patients in the training and validation sets

Characteristic	Training set (88 patients)	Validation set (99 patients)	*P* value
Age (y), median (IQR)	61 (56–66)	59 (52–64)	0.04
Male, *n* (%)	70 (80%)	78 (79%)	1.00
Aetiology of chronic liver disease, *n* (%)			
Hepatitis C virus	43 (49%)	70 (71%)	<0.001
Hepatitis B virus	25 (28%)	23 (23%)	0.50
Alcohol	17 (19%)	18 (18%)	0.85
Non-alcoholic fatty liver diseases	3 (3%)	0 (0%)	0.10
Albumin (g/dl), median (IQR)	3.7 (3.5–3.9)	3.8 (3.5–4.1)	0.09
Bilirubin (mg/dl), median (IQR)	0.8 (0.7–1.2)	1.0 (0.8–1.4)	0.01
Platelet count $\times$ 10^3/mm^3, median (IQR)	136 (97–173)	134 (84–204)	0.64
Child Pugh score*, median (IQR)	5 (5–6)	5 (5–6)	0.68
Child Pugh class, *n* (%)			
A	84 (95%)	87 (89%)	0.11
B	4 (5%)	11 (11%)	
Tumour size (cm), median (IQR)	2.3 (2.0–2.9)	2.2 (1.8–3.0)	0.63
Tumour number, *n* (%)			
Single	74 (84%)	73 (84%)	0.09
Multiple	14 (16%)	14 (14%)	
Presence of satellite lesions	12 (13%)	16 (16%)	0.54
α-foetoprotein (ng/ml), median (IQR)	16 (4.0–88.8)	37 (10–197)	0.009
>400 ng/ml, *n* (%)	7 (8%)	15 (15%)	0.17
AJCC stage, *n* (%)			
I/II	65/23 (74%/26%)	72/14 (82%/16%)	0.62
IIIA	0 (0%)	2 (2%)	
BCLC stage, *n* (%)			
0/A	12/75 (14%/85%)	23/59 (26%/67%)	0.12
B	1 (1%)	6 (7%)	

AJCC, American Joint Committee on Cancer'; BCLC, Barcelona Clinic Liver Cancer; HCC, hepatocellular carcinoma.
*Child-Pugh score was unavailable for one patient in the validation set.

pathological features (Table S5). Discordant determination was resolved by discussion among all evaluators and a consensus diagnosis was reached. There was no significant difference in their prevalence between the training and validation sets except for the pseudoglandular pattern and the clear cell variant, which were more frequently observed in the training set. The microtrabecular pattern was the most prevalent feature observed in more than half of the tumours, followed by the macrotrabecular/compact pattern observed in approximately 40% of the tumours. SH-HCC was observed in approximately 20% in both training and validation sets. We confirmed correlation of the SH-HCC variant with presence of steatosis and steatohepatitis in background liver as reported in previous studies (Table S6) (40). Presence of cirrhosis was not associated with the SH-HCC variant ($P = 0.52$). Relatively higher immune cell infiltrates (score of 2) were observed in approximately 40% to 50% of the tumours. Osteoclast-like cells were observed in 6 and 2 tumours in the training and validation sets, respectively, and accumulated in S1 and S2 subclasses, representing higher grade tumours. Chromophobe HCC was not observed in the current patient series, which may be due to the earlier tumour stage (median tumour size 2.3 cm and 2.2 cm in the training and validation sets respectively) compared to the tumours in the original report of the variant (median tumour size 5.7 cm) (31). Fatty change had similar occurrence in the two sets, whereas the clear cell variant was more prevalent in the training set. More than 80% of the tumours were of Edmondson-Steiner grade I or II.

Molecular deregulations associated with histopathological features of HCC tumours

The distinct histopathological features with significant correlation with the molecular subclasses suggest that molecular pathway deregulations are related to formation of the morphological features. The microtrabecular pattern is characterized by retained normal hepatocyte functions involved in a variety of metabolic pathways and enrichment of gene signatures implicated in better HCC prognosis and biologically less aggressive molecular subclasses, including the S3 subclass (41–43) (Tables S4 and S7). The macrotrabecular/compact pattern was associated with accelerated cell cycle progression and cell proliferation, activation of an oncogene *YAP* recently implicated in HCC (44) as determined by induction of pathway target genes. The Yap target genes were similarly activated in the S2 subclass (Fig. S3), and induction of genes regulated by transcription factors, *E2F1* and *MYC*. The S2 subclass

Table 2. Histopathological features and HCC molecular subclasses in the training and validation sets

	Training set (96 HCC tumours)	Validation set (99 HCC tumours)	*P* value
Histopathological feature			
Architectural pattern			
Microtrabecular	53 (55%)	53 (54%)	0.89
Macrotrabecular/ compact	38 (40%)	39 (39%)	1.00
Pseudoglandular	31 (32%)	14 (14%)	0.004
Cytological variant			
SH-HCC	19 (20%)	17 (17%)	0.71
Clear cell	23 (24%)	7 (7%)	0.001
Fatty change	17 (18%)	10 (10%)	0.15
Edmondson-Steiner grade			
I	12 (13%)	21 (21%)	0.29
II	66 (69%)	62 (63%)	
III	17 (18%)	16 (16%)	
IV	1 (1%)	0 (0%)	
Immune cell infiltrate score*			
0	15 (16%)	18 (18%)	0.08
1	42 (44%)	28 (28%)	
2	39 (41%)	53 (54%)	
Microvascular invasion	9 (9%)	16 (16%)	0.20
Molecular subclass			
S1	30 (31%)	30 (30%)	0.46
S2	27 (28%)	21 (21%)	
S3	39 (41%)	48 (48%)	

HCC, hepatocellular carcinoma; OR, odds ratio; CI, confidence interval; SH-HCC, steatohepatitic HCC; AFP, alpha-foetoprotein.

*Immune cell infiltrate score, 0: 0–5 cells, 1: 5–20 cells, 2: >20 cells.

signature together with published liver cancer signatures of biologically aggressive subclasses (41–43), stemness markers *EPCAM/KRT19*, MET activation, vascular invasion, and poor prognosis were strikingly induced. The S1 subclass signature and TGF-beta signature were also enriched to lesser extent. Two gene regulatory modules (no. 15 and no. 22) were associated with the macrotrabecular/compact pattern with key driver genes, *PCNA* and *BIRC5* (also known as survivin), implicated in cellular proliferation in HCC (Tables S8 and S9; Fig. S4A, B) (45). The pseudoglandular pattern was associated with a gene signature of HCC tumour harbouring *CTNNB1* exon 3 mutations accompanied by the overexpression of liver-specific WNT target genes such as *GLUL* (42, 43). *BMP4*, which is known to be involved in prostate gland formation under regulation by CTNNB1 pathway (46, 47), was identified as a key driver gene in a gene regulatory module (no. 56) associated with the pseudoglandular pattern (Tables S8 and S9; Fig. S5). The SH-HCC variant was associated with activation of *YAP* oncogene and several kinases, including STK33, KRAS, and RAF, and pathways involved in collagen formation and extracellular matrix organization. In fact, *CXCL12*, ligand of a chemokine receptor CXCR4 involved in hepatic fibrosis (48, 49), was identified as a key driver gene for the SH-HCC variant together with genes encoding collagens (*COL1A2*, *COL3A1*, and *COL6A2*) (Tables S8 and S9; Fig. S6). A CXCR4 inhibitor, AMD3100, was recently reported to inhibit intra-tumoral fibrogenesis induced by a multikinase inhibitor, sorafenib (50). The S1 subclass signature was significantly induced in the SH-HCC variant together with signature of Chiang08 subclass Proliferation (43), further supporting our correlation analysis with logistic regression (Table 3). Clear cell variant was significantly associated with signatures of the S2 subclass, biologically more aggressive HCC tumours (41, 42), *EPCAM/KRT19*, and cholangiocarcinoma stem cell (Tables S4 and S7; Table 3). These findings collectively provide

Table 3. Tumour-related clinicopathological features associated with HCC molecular subclasses in the training set (logistic regression)

	Univariable analysis			Multivariable analysis	
Variable	No. of HCC tumours (%)	OR (95% CI)	*P* value	OR (95% CI)	*P* value
S1 subclass	S1: $n = 30$/Rest: $n = 66$				
SH-HCC	11 (37%)/8 (12%)	4.20 (1.47–11.97)	0.007	4.25 (1.44–13.20)	0.01
Immune cell infiltrate ≥2	18 (60%)/21 (32%)	3.21 (1.31–7.87)	0.01	3.25 (1.29–8.53)	0.01
S2 subclass	S2: $n = 27$/Rest: $n = 69$				
Microtrabecular	4 (15%)/49 (71%)	0.07 (0.02–0.23)	<0.001		
Macrotrabecular/compact	22 (81%)/16 (23%)	14.58 (4.75–44.69)	<0.001	11.99 (3.48–41.24)	<0.001
Pseudoglandular	2 (7%)/29 (42%)	0.11 (0.02–0.50)	0.004	0.22 (0.04–1.16)	0.07
Clear cell	14 (52%)/9 (13%)	7.18 (2.56–20.11)	<0.001		
Serum AFP >400 ng/ml	6 (22%)/2 (3%)	9.57 (1.80–51.03)	0.008	10.81 (1.27–91.63)	0.03
S3 subclass	S3: $n = 39$/Rest: $n = 57$				
Microtrabecular	32 (82%)/21 (37%)	7.84 (2.94–20.86)	<0.001	3.94 (1.23–12.56)	0.02
Macrotrabecular/compact	6 (15%)/32 (56%)	0.14 (0.05–0.39)	<0.001		
Pseudoglandular	19 (49%)/11 (19%)	3.56 (1.46–8.71)	0.005		
SH-HCC	1 (3%)/18 (32%)	0.06 (0.01–0.45)	0.006	0.05 (0.01–0.44)	0.007
Clear cell	3 (8%)/20 (35%)	0.15 (0.04–0.56)	0.005	0.20 (0.05–0.91)	0.04
Edmondson-Steiner I or II	36 (92%)/42 (74%)	4.29 (1.15–16.00)	0.03	3.08 (0.65–14.58)	0.16

HCC, hepatocellular carcinoma; OR, odds ratio; CI, confidence interval; SH-HCC, steatohepatitic HCC; AFP, alpha-foetoprotein.

comprehensive overview of molecular deregulations, biomarkers, and/or potential therapeutic targets underlying the distinct histopathological features that can be further pursued in subsequent studies.

Determination of HCC molecular subclasses in the training set

We next determined the HCC molecular subclasses in the training set using a clinically applicable and inexpensive assay. From among 103 HCC tumour samples/foci from 95 patients in the training set, 96 foci (93%) from 88 patients yielded good quality RNA for the expression profiling (Fig. S1). By using the molecular subclass prediction model and algorithm from our previous study without any modification, 30 (31%), 27 (28%) and 39 (41%) samples in the training set were classified into S1, S2, S3 subclasses respectively (Table 2; Fig. 1B). Prevalence of the predicted molecular subclasses was highly comparable to the results in previous studies by us and others (5, 6), indicating robust performance of the 30-gene signature assay. The highest serum AFP level in the S2 subclass, which was identified in our previous study (5), was replicated in the training set of this study ($P < 0.001$) (Fig. S7), further supporting validity of the assay.

Correlation of clinicopathological features with HCC molecular subclasses

We next sought to determine tumour-related clinicopathological variables associated with the molecular subclasses determined by the 30-gene signature assay. Univariable logistic regression revealed several striking correlations between the clinicopathological features and the HCC molecular subclasses (Fig. S8A, B, Table 3). The positive correlations of HBV infection and *EPCAM* overexpression with the S2 subclass identified in our previous study were confirmed (5). Presence of the SH-HCC variant and higher immune cell infiltrates were significantly associated with the S1 subclass. Lack of the microtrabecular and the pseudoglandular patterns, presence of the macrotrabecular/compact pattern, the clear cell variant, and high serum AFP level were associated with the S2 subclass. Presence of the microtrabecular or the pseudoglandular pattern, absence of the macrotrabecular/compact pattern and the clear cell and the SH-HCC variants, and lower Edmondson-Steiner grade were associated with the S3 subclass. In multivariable modelling, both SH-HCC variant and immune cell infiltrates remained significant for association with the S1 subclass (Table 3). Association of the macrotrabecular/compact pattern and high serum AFP with the S2 subclass remained significant. The microtrabecular pattern, absence of the SH-HCC and the clear cell variants were significantly associated with the S3 subclass. These results suggest that HCC molecular subclasses can be estimated reasonably well based on assessment of the clinicopathological features. We next assessed whether molecular subclass was associated with previously published markers of hepatocarcinogenesis (51, 52) (*GLUL*, *GPC3*, *LYVE1* and *BIRC5*) as implemented in the EASL guidelines (53). We identified a positive association between *GPC3* high expression and S2 subclass in both the training and validation sets. In the validation set, high expression of *BIRC5* was associated with S1 subclass, and high expression of *LYVE1* and *GLUL* were associated with S3 subclass (Fig. S8A, B). Additionally, we assessed the association between HCC molecular subclass and patient prognosis, but there was no significant association with survival or recurrence both in training and validation sets (Table S10). This is consistent with our previous observation, in which tumour-derived molecular information had no prognostic association, where the majority of the tumours are in early stage (BCLC 0/A) and recurrent tumours were clonally unrelated with the resected primary tumours (54).

Clinicopathological indices predictive of HCC molecular subclasses

Based on the significant correlations of the clinicopathological features with the molecular subclasses, we con-

Table 4. Performance of the clinicopathological indices predictive of HCC molecular subclasses (optimized for PPV)

	Training set					Validation set				
Molecular subclass	AUROC	PPV (%)	NPV (%)	Sensitivity (%)	Specificity (%)	AUROC	PPV (%)	NPV (%)	Sensitivity (%)	Specificity (%)
S1	0.69	89	75	27	98	0.71	60	73	20	94
S2	0.86	80	75	15	99	0.77	50	82	24	94
S3	0.83	71	79	69	81	0.73	71	69	65	75

HCC, hepatocellular carcinoma; AUROC, area under receiver operating characteristic curve; PPV, positive predictive value; NPV, negative predictive value; SH-HCC, steatohepatitic HCC; AFP, alpha-foetoprotein.

Molecular subclass prediction was performed using the following formulae and cut-off values optimized for PPV in the training set:

S1 = 1.45 × SH-HCC (0: no, 1: yes) + 1.18 × Immune cell infiltrate (0: 0–1, 1: 2); >2.04 was predicted as S1 subclass.

S2 = 2.48 × Macrotrabecular/compact (0: no, 1: yes) + 2.38 × serum AFP (0: ≤400 ng/ml; 1: >400 ng/ml) – 1.5 × pseudoglandular (0: no, 1: yes); >3.67 was predicted as S2 subclass.

S3 = 1.37 × Microtrabecular (0: no, 1: yes) – 2.97 × SH-HCC (0: no, 1: yes) – 1.59 × clear cell (0: no, 1: yes) + 1.13 × tumour grade (0: Edmondson-Steiner III or IV, 1: Edmondson-Steiner I or II); >1.94 was predicted as S3 subclass.

structed a prediction index for each subclass using the regression coefficients from the multivariable logistic regression models (see footnote of Table 4). In the training set, the area under ROC curve (AUROC) for the S1, S2 and S3 subclasses were 0.69, 0.87, and 0.85, respectively, based on which cut-off value for each predictive index was determined (Table 4; Fig. S9). Each prediction index and corresponding cut-off value was evaluated in the validation set without making any modification. The validation set yielded comparable AUROC of 0.71, 0.79 and 0.73 for the S1, S2 and S3 subclasses respectively. With the cut-off values optimized for PPV in the training set, S1, S2, and S3 subclasses in the validation set were predicted with PPVs of 60%, 50%, and 71% respectively. Based on the cut-off values for sensitivity/specificity, all subclasses were predicted with sensitivity greater than 80% and negative predictive value nearly equal to or greater than 80% (Table S11). Based on the PPVs in the validation set and ORRs ranging from 50% to 70% assumed from previously conducted phase 2 and 3 trials of molecular targeted agents in molecular subtype-enriched lung cancer patients (39), sample sizes required to detect therapeutic benefit were reduced by 59–79%, and NNTs were reduced by 37–50% compared to a strategy enrolling 'all comers' without enrichment for a specific molecular subclass (Fig. S10, Table S12).

Discussion

It is increasingly recognized that molecular biomarkers will play the key role in design and conduct of more cost-effective and expedited drug development and evaluation in clinical trials. Despite the urgent unmet need, predictive biomarker-enriched clinical trials are rarely conducted because pharmaceutical companies rarely fund the biomarker component of the trials. This issue could be resolved if clinically meaningful enrichment of specific molecular subtype is feasible by using clinically readily available predictive indices, which enable better powered clinical trial not to miss therapeutic benefit. This financial constraint is more relevant in resource-poor countries, where more than 80% of HCC patients are diagnosed. Our current study showed encouraging results as a proof of concept, demonstrating that clinical variable-based estimation of molecular subtype is a viable approach to meet this need. This strategy will also benefit other pathogen-induced cancers prevalent in developing regions of the world.

A byproduct of this study is a clinically applicable HCC molecular classification assay. Transcriptome-based clinical diagnostic development has been a challenging task because of poor reproducibility of the assay measurements because of artefacts introduced during the process of target gene amplification, which have required centralized reference laboratories to perform the assay for rigorous quality control (55). The digital transcript counting technology without target gene amplification adapted in this study is expected to overcome the issue. It is also worth noting that the assay is applicable even for severely degraded RNA isolated from real-world archived FFPE tissue sections (17). The cost for clinical assay development is a prohibitive factor in developing companion biomarkers for each molecular targeted therapy, which will easily overtax currently available biomedical and financial resources. Broadly applicable biomarkers, such as our proposed molecular classification of HCC, could eliminate such efforts and enable more cost-effective drug development and biomarker-guided clinical trials.

Prognostic implication of histopathological features has been studied over the past decades in numerous studies (56). However, no histopathological feature of HCC has been incorporated in the prognostic staging systems because of unsatisfactory reproducibility (57). For example, prognostic association of the clear cell variant has been controversial despite its unambiguous pathological diagnostic criteria (Table S13). Similarly, we observed that prognostic association of HCC molecular subclasses in literature hugely varies across studies despite obvious presence of the subclasses (33). Recent studies suggest that this is likely because of diversity of the disease stage represented in each study, i.e. even if a tumour harbours a more aggressive molecular phenotype, the tumour has less chance to disseminate and impact patient survival if it is diagnosed at an earlier stage and successfully treated, whereas persisting cirrhosis and *de novo* HCC arisen from the cirrhotic liver have more influence on the prognosis independent of the successfully treated initial primary tumour (33). The current study revealed surprisingly close correlation between histopathological features and molecular subclasses that links these independent observations on prognostic association of histopathological or molecular features. This finding highlights the importance to assess prognostic implication of histopathological and molecular HCC tumour characteristics according to the disease stage to elucidate their clinical utility.

The incidence and prevalence of NAFLD/NASH are increasing worldwide (58). Epidemiological studies suggest that there are carcinogenic mechanisms unique to NASH (59). The SH-HCC variant is a unique feature tightly linked to the presence of steatosis and steatohepatitis in the background liver (40). Formation of this variant may provide mechanistic insights into NASH-induced HCC development that involves specific molecular pathways such as CXCL12/CXCR4-related extracellular matrix production, because of the presence of and/or genetic susceptibility to NASH. Also, it will be of interest to evaluate if SH-HCC is associated with more disseminative phenotype as seen in the S1 tumours (5) when the patients are longitudinally followed up.

In conclusion, we have successfully developed clinically readily applicable clinicopathological predictive

indices of HCC molecular classification. Histopathological features of HCC tumour are accompanied by distinct molecular pathway deregulations and could also serve as surrogate markers of HCC molecular subclasses. This observation demonstrates a proof of concept that can be further pursued with refined molecular classification or other types of molecular characterization in future studies. The clinicopathological indices as well as the clinically applicable assay will serve as tools that enable wider access to the molecular information for the clinical and translational research communities to further explore therapeutic implication of the molecular characteristics of HCC, and could potentially contribute to a substantial improvement of the dismal prognosis of HCC.

Acknowledgements

The nCounter Elements assay was performed at Mount Sinai qPCR Shared Resource Facility. Bioinformatics analysis was performed by using High Power Computing facility at Mount Sinai Genomics Core and Department of Scientific Computing.

Financial support: This research was supported by Uehara Memorial Foundation (to SN), FLAGS foundation, Nuovo-Soldati Cancer Research Foundation, and advanced training grant from Geneva University Hospital (to NG), and National Institute of Health (DK099558) and the Irma T. Hirschl Trust (to YH).

Conflict of interest: The authors do not have any disclosures to report.

References

1. Hoshida Y, Fuchs BC, Bardeesy N, Baumert TF, Chung RT. Pathogenesis and prevention of hepatitis C virus-induced hepatocellular carcinoma. *J Hepatol* 2014; **60**: S79–90.
2. Llovet JM, Ricci S, Mazzaferro V, *et al.* Sorafenib in advanced hepatocellular carcinoma. *N Engl J Med* 2008; **359**: 378–90.
3. Cheng AL, Kang YK, Chen Z, *et al.* Efficacy and safety of sorafenib in patients in the Asia-Pacific region with advanced hepatocellular carcinoma: a phase III randomised, double-blind, placebo-controlled trial. *Lancet Oncol* 2009; **10**: 25–34.
4. Llovet JM, Hernandez-Gea V. Hepatocellular carcinoma: reasons for phase III failure and novel perspectives on trial design. *Clin Cancer Res* 2014; **20**: 2072–9.
5. Hoshida Y, Nijman SM, Kobayashi M, *et al.* Integrative transcriptome analysis reveals common molecular subclasses of human hepatocellular carcinoma. *Cancer Res* 2009; **69**: 7385–92.
6. Kan Z, Zheng H, Liu X, *et al.* Whole-genome sequencing identifies recurrent mutations in hepatocellular carcinoma. *Genome Res* 2013; **23**: 1422–33.
7. Turato C, Vitale A, Fasolato S, *et al.* SERPINB3 is associated with TGF-beta1 and cytoplasmic beta-catenin expression in hepatocellular carcinomas with poor prognosis. *Br J Cancer* 2014; **110**: 2708–15.
8. Goossens N, Sun X, Hoshida Y. Molecular classification of hepatocellular carcinoma: potential therapeutic implications. *Hepat Oncol* 2015; **60**: S79–90.
9. Giannelli G, Villa E, Lahn M. Transforming growth factor-beta as a therapeutic target in hepatocellular carcinoma. *Cancer Res* 2014; **74**: 1890–4.
10. Zhu AX, Gold PJ, El-Khoueiry AB, *et al.* First-in-man phase I study of GC33, a novel recombinant humanized antibody against glypican-3, in patients with advanced hepatocellular carcinoma. *Clin Cancer Res* 2013; **19**: 920–8.
11. Santoro A, Rimassa L, Borbath I, *et al.* Tivantinib for second-line treatment of advanced hepatocellular carcinoma: a randomised, placebo-controlled phase 2 study. *Lancet Oncol* 2013; **14**: 55–63.
12. Hong Y, Peng Y, Guo ZS, *et al.* Epitope-optimized alpha-fetoprotein genetic vaccines prevent carcinogen-induced murine autochthonous hepatocellular carcinoma. *Hepatology* 2014; **59**: 1448–58.
13. Finn RS, Aleshin A, Dering J, *et al.* Molecular subtype and response to dasatinib, an Src/Abl small molecule kinase inhibitor, in hepatocellular carcinoma cell lines in vitro. *Hepatology* 2013; **57**: 1838–46.
14. Deshmukh M, Hoshida Y. Genomic profiling of cell lines for personalized targeted therapy for hepatocellular carcinoma. *Hepatology* 2013; **58**: 2207.
15. Fitamant J, Kottakis F, Benhamouche S, *et al.* YAP inhibition restores hepatocyte differentiation in advanced HCC leading to tumor regression. *Cell Rep* 2015; **10**: S2211–1247.
16. Easl-Eortc. EASL-EORTC clinical practice guidelines: management of hepatocellular carcinoma. *J Hepatol* 2012; **56**: 908–43.
17. Kojima K, April C, Canasto-Chibuque C, *et al.* Transcriptome profiling of archived sectioned formalin-fixed paraffin-embedded (AS-FFPE) tissue for disease classification. *PLoS ONE* 2014; **9**: e86961.
18. Chalasani N, Younossi Z, Lavine JE, *et al.* The diagnosis and management of non-alcoholic fatty liver disease: practice guideline by the American Gastroenterological Association, American Association for the Study of Liver Diseases, and American College of Gastroenterology. *Gastroenterology* 2012; **142**: 1592–609.
19. Goodman ZD. Neoplasms of the liver. *Mod Pathol* 2007; **20**(Suppl 1): S49–60.
20. Macsween RNM, Burt AD, Portmann B, Ferrell LD, Sciencedirect (Online Service). *MacSween's Pathology of the Liver*, 6th edn. Edinburgh: Churchill Livingstone, 2011; 1 online resource (1 v.).
21. Bosman FT, World Health Organization, International Agency for Research on Cancer. *WHO Classification of Tumours of the Digestive System*, 4th edn. Lyon: International Agency for Research on Cancer, 2010.
22. Wu PC, Lai CL, Lam KC, Lok AS, Lin HJ. Clear cell carcinoma of liver. An ultrastructural study. *Cancer* 1983; **52**: 504–7.
23. Audisio RA, Bombelli L, Lombardi L, Andreola S. A clinico-pathologic study of clear-cell hepatocellular carcinoma. *Tumori* 1987; **73**: 389–95.
24. Yang SH, Watanabe J, Nakashima O, Kojiro M. Clinicopathologic study on clear cell hepatocellular carcinoma. *Pathol Int* 1996; **46**: 503–9.
25. Salomao M, Yu WM, Brown RS Jr, Emond JC, Lefkowitch JH. Steatohepatitic hepatocellular carcinoma (SH-HCC): a distinctive histological variant of HCC in hepatitis C

virus-related cirrhosis with associated NAFLD/NASH. *Am J Surg Pathol* 2010; **34**: 1630–6.
26. Jain D, Nayak NC, Kumaran V, Saigal S. Steatohepatitic hepatocellular carcinoma, a morphologic indicator of associated metabolic risk factors: a study from India. *Arch Pathol Lab Med* 2013; **137**: 961–6.
27. Shibahara J, Ando S, Sakamoto Y, Kokudo N, Fukayama M. Hepatocellular carcinoma with steatohepatitic features: a clinicopathological study of Japanese patients. *Histopathology* 2014; **64**: 951–62.
28. Edmondson HA, Steiner PE. Primary carcinoma of the liver: a study of 100 cases among 48,900 necropsies. *Cancer* 1954; **7**: 462–503.
29. Kleiner DE, Brunt EM, Van Natta M, *et al.* Design and validation of a histological scoring system for nonalcoholic fatty liver disease. *Hepatology* 2005; **41**: 1313–21.
30. Unitt E, Marshall A, Gelson W, *et al.* Tumour lymphocytic infiltrate and recurrence of hepatocellular carcinoma following liver transplantation. *J Hepatol* 2006; **45**: 246–53.
31. Wood LD, Heaphy CM, Daniel HD, *et al.* Chromophobe hepatocellular carcinoma with abrupt anaplasia: a proposal for a new subtype of hepatocellular carcinoma with unique morphological and molecular features. *Mod Pathol* 2013; **26**: 1586–93.
32. Ikeda T, Seki S, Maki M, *et al.* Hepatocellular carcinoma with osteoclast-like giant cells: possibility of osteoclastogenesis by hepatocyte-derived cells. *Pathol Int* 2003; **53**: 450–6.
33. Hoshida Y, Toffanin S, Lachenmayer A, *et al.* Molecular classification and novel targets in hepatocellular carcinoma: recent advancements. *Semin Liver Dis* 2010; **30**: 35–51.
34. Subramanian A, Tamayo P, Mootha VK, *et al.* Gene set enrichment analysis: a knowledge-based approach for interpreting genome-wide expression profiles. *Proc Natl Acad Sci U S A* 2005; **102**: 15545–50.
35. Zhang B, Gaiteri C, Bodea LG, *et al.* Integrated systems approach identifies genetic nodes and networks in late-onset Alzheimer's disease. *Cell* 2013; **153**: 707–20.
36. Song WM, Di Matteo T, Aste T. Nested hierarchies in planar graphs. *Discrete Appl Math* 2011; **159**: 2135–46.
37. Song WM, Di Matteo T, Aste T. Building complex networks with Platonic solids. *Phys Rev E Stat Nonlin Soft Matter Phys* 2012; **85**(4 Pt 2): 046115.
38. Tran LM, Zhang B, Zhang Z, *et al.* Inferring causal genomic alterations in breast cancer using gene expression data. *BMC Syst Biol* 2011; **5**: 121.
39. Stinchcombe TE. Recent advances in the treatment of non-small cell and small cell lung cancer. *F1000prime Rep* 2014; **6**: 117.
40. Salomao M, Remotti H, Vaughan R, *et al.* The steatohepatitic variant of hepatocellular carcinoma and its association with underlying steatohepatitis. *Hum Pathol* 2012; **43**: 737–46.
41. Lee JS, Chu IS, Heo J, *et al.* Classification and prediction of survival in hepatocellular carcinoma by gene expression profiling. *Hepatology* 2004; **40**: 667–76.
42. Boyault S, Rickman DS, De Reynies A, *et al.* Transcriptome classification of HCC is related to gene alterations and to new therapeutic targets. *Hepatology* 2007; **45**: 42–52.
43. Chiang DY, Villanueva A, Hoshida Y, *et al.* Focal gains of VEGFA and molecular classification of hepatocellular carcinoma. *Cancer Res* 2008; **68**: 6779–88.
44. Perra A, Kowalik MA, Ghiso E, *et al.* YAP activation is an early event and a potential therapeutic target in liver cancer development. *J Hepatol* 2014; **61**: 1088–96.
45. Ito T, Shiraki K, Sugimoto K, *et al.* Survivin promotes cell proliferation in human hepatocellular carcinoma. *Hepatology* 2000; **31**: 1080–5.
46. Prins GS, Putz O. Molecular signaling pathways that regulate prostate gland development. *Differentiation* 2008; **76**: 641–59.
47. Mehta V, Schmitz CT, Keil KP, *et al.* Beta-catenin (CTNNB1) induces Bmp expression in urogenital sinus epithelium and participates in prostatic bud initiation and patterning. *Dev Biol* 2013; **376**: 125–35.
48. Ding BS, Cao Z, Lis R, *et al.* Divergent angiocrine signals from vascular niche balance liver regeneration and fibrosis. *Nature* 2014; **505**: 97–102.
49. Hong F, Tuyama A, Lee TF, *et al.* Hepatic stellate cells express functional CXCR4: role in stromal cell-derived factor-1alpha-mediated stellate cell activation. *Hepatology* 2009; **49**: 2055–67.
50. Chen Y, Huang Y, Reiberger T, *et al.* Differential effects of sorafenib on liver versus tumor fibrosis mediated by stromal-derived factor 1 alpha/C-X-C receptor type 4 axis and myeloid differentiation antigen-positive myeloid cell infiltration in mice. *Hepatology* 2014; **59**: 1435–47.
51. Llovet JM, Chen Y, Wurmbach E, *et al.* A molecular signature to discriminate dysplastic nodules from early hepatocellular carcinoma in HCV cirrhosis. *Gastroenterology* 2006; **131**: 1758–67.
52. Di Tommaso L, Franchi G, Park YN, *et al.* Diagnostic value of HSP70, glypican 3, and glutamine synthetase in hepatocellular nodules in cirrhosis. *Hepatology* 2007; **45**: 725–34.
53. European Association for the Study of the Liver. EASL-EORTC clinical practice guidelines: management of hepatocellular carcinoma. *J Hepatol* 2012; **56**: 908–43.
54. Hoshida Y, Villanueva A, Kobayashi M, *et al.* Gene expression in fixed tissues and outcome in hepatocellular carcinoma. *N Engl J Med* 2008; **359**: 1995–2004.
55. Koscielny S. Why most gene expression signatures of tumors have not been useful in the clinic. *Sci Transl Med* 2010; **2**: 14 ps2.
56. Tandon P, Garcia-Tsao G. Prognostic indicators in hepatocellular carcinoma: a systematic review of 72 studies. *Liver Int* 2009; **29**: 502–10.
57. Bruix J, Sherman M. Management of hepatocellular carcinoma: an update. *Hepatology* 2011; **53**: 1020–2.
58. Lazo M, Hernaez R, Eberhardt MS, *et al.* Prevalence of nonalcoholic fatty liver disease in the United States: the Third National Health and Nutrition Examination Survey, 1988–1994. *Am J Epidemiol* 2013; **178**: 38–45.
59. Michelotti GA, Machado MV, Diehl AM. NAFLD, NASH and liver cancer. *Nat Rev Gastroenterol Hepatol* 2013; **10**: 656–65.

Supporting information

Additional Supporting Information may be found at onlinelibrary.wiley.com/doi/10.1111/liv.12889/suppinfo